N91-24408

IV. MICROSTRUCTURAL EVOLUTION DURING AGING OF AN Al-Cu-Li-Ag-Mg-Zr ALLOY

K.S. Kumar, S.A. Brown, and J.R. Pickens

I. INTRODUCTION

Alloys in the Al-Cu-Li Ag-Mg subsystems have been developed that exhibit desirable combinations of strength and ductility (1). These "Weldalite™" alloys, are unique for Al-Cu-Li alloys in that with or without a prior cold stretching operation, they obtain excellent strength-ductility combinations upon natural and artificial aging. This is significant because it enables complex, near-net shape products such as forgings and super-plastically-formed parts to be heat treated to ultra-high strengths. On the other hand, commercial extrusions, rolled plates and sheets of other Al-Cu-Li alloys are typically subjected to a cold-stretching operation before artificial aging to the highest strength tempers to introduce dislocations that provide low-energy nucleation sites for strengthening precipitates such as the T_1 phase (2,3).

The variation in yield strength (YS) with Li content in the near-peak aged condition for these Weldalite™ alloys was examined (4) and a peak in strength was observed at ~1.3 wt% Li. The associated microstructures were examined and it was proposed that the significant decrease in strength for alloys with Li content >1.3 wt% was due to the formation of δ' at the expense of the more potent strengthening phase T_1. Subsequently, research interest has centered around the "Weldalite™ 049" alloy which contains a nominal 1.3 wt. % Li. Microstructural development in Weldalite™ 049 with artificial aging has been reported, with and without a prior stretching operation (5-7). The ultra-high strength observed in this alloy in the peak-aged tempers (T6, T8) was attributed primarily to the homogeneously distributed fine T_1 phase, (4,5) although some θ' and S' were also observed (5,7). It was suggested that Ag, Mg and Zr may aid in trapping excess vacancies, thereby providing low energy nucleation sites for the precipitation of T_1, and discouraging lattice diffusion which decreases precipitate growth (5).

In this study, the microstructure in the naturally aged condition, as well as upon artificial aging for various times along the aging curve (Figure 1), has been examined for a Weldalite™ alloy containing a relatively high Li level (1.7 wt. %). The effect of a 3% stretch, prior to aging but immediately after solution treatment, on the resulting microstructure is reported. It is hoped that this study will allow the identification of processing parameters that can be modified to further improve the

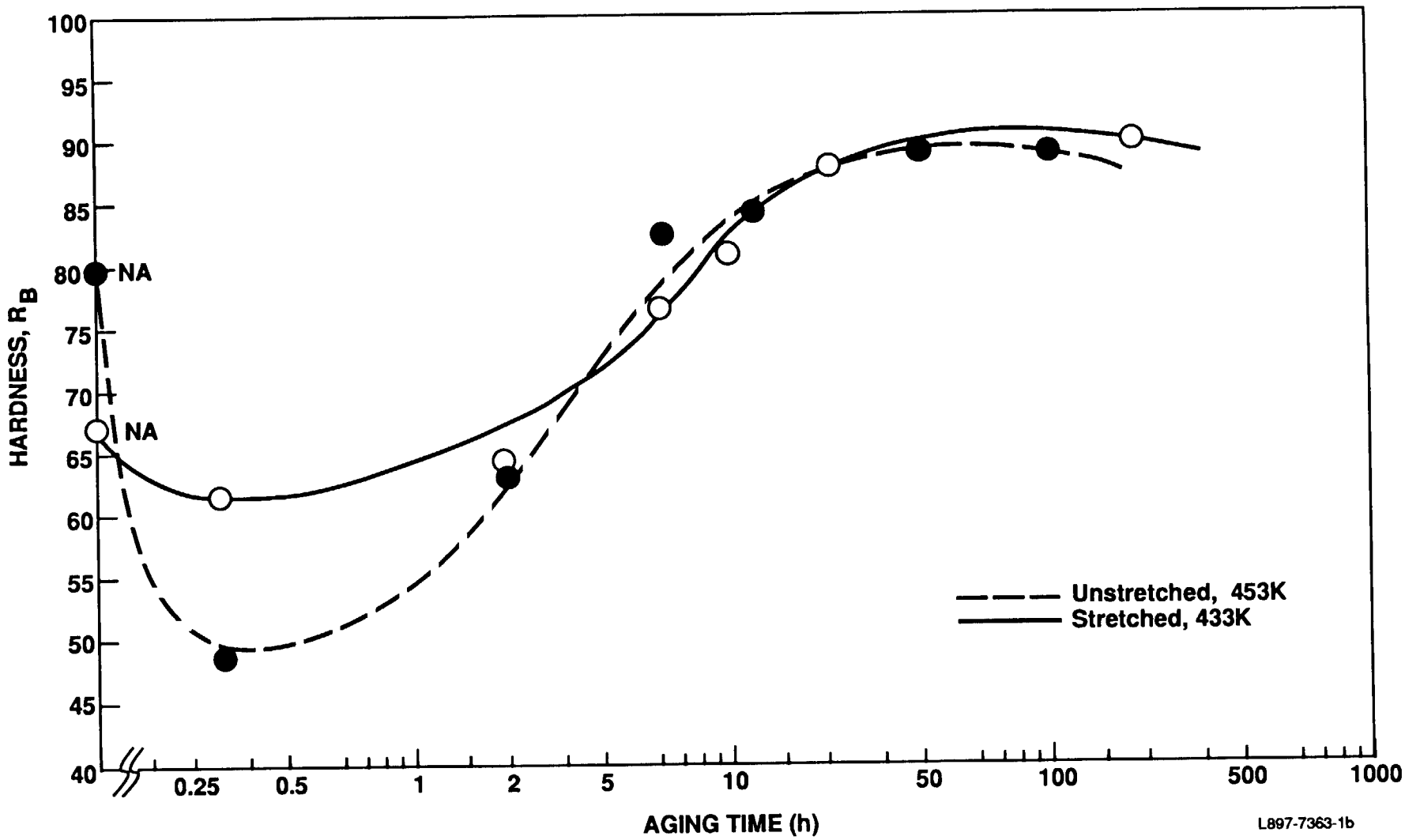

Figure 1 Isothermal aging response of the stretched and unstretched material at 433K and 453K respectively.

strength of this alloy which is more attractive than the 1.3 wt. % Li-containing alloy from a density point of view.

In such complex alloys, several metastable phases precipitate during aging. The crystallographic characteristics of these precipitates and the relationships they bear with the matrix are reviewed in the next section to provide the background for understanding the results obtained in this study.

2. PRECIPITATE CHARACTERISTICS IN THE Al-Cu-Li-Ag-Mg-Zr SYSTEM

The types of precipitates observed in such a complex system can be primarily divided into two categories. The first type are those that are stable equilibrium phases, their presence being determined by the alloy composition and the heat-treatment condition. These include binary phases such as Al_2Cu (θ), AlLi (δ), Al_3Zr (DO_{22}-type) and ternary precipitates like T_1(Al_2CuLi), T_2 (Al_6CuLi_3), T_B (Al_7LiCu_4), R(Al_5Li_3Cu) and S (Al_2CuMg). A large quantity of these primary phases, present from the cast and homogenized condition dissolve during the solutionizing treatment and are retained in supersaturated solid solution upon quenching, providing the driving force for precipitation of metastable phases upon subsequent aging. To maximize the alloy's capabilities in terms of its mechanical properties, it is critical to optimize the solution treatment temperature and time. Certain alloy compositions dictate the presence of excess primary phases even after optimal heat-treatment and in these cases some primary phases are carried through the entire thermal processing schedule. Whereas these primary phases, depending on the size, shape, and volume fraction can be deleterious to mechanical properties, especially toughness, they may enhance weldability (8).

While these primary phases are important, of greater significance to this paper are the metastable phases that result during aging. A list of these phases together with their morphology and habit planes is provided in Table I.

Since so many different metastable phases can be present in such alloys during aging, the corresponding SAD patterns tend to be complex. In this paper, the precipitation sequence has been characterized using SAD patterns predominantly with a [100], [110] or [112] matrix zone axis and the diffraction spots and streaks from these various

precipitates for the above orientations of the matrix are shown schematically in Figure 2.

Table I: Metastable Phases Found in the Al-Cu-Li-Ag-Mg-Zr System

Precipitate	Morphology	Habit Plane
(Al_3Zr)	Spherical	--
$\delta'(Al_3Li)$	Spherical	- -
GP Zones (Al-Cu)	Clusters	- -
$\theta'(Al_2Cu)$	Discs	{100}
$T_1(Al_2CuLi)$	Platelet	{111}
Ω(Al-Cu-Ag-Mg?)	Platelet	{111}
$S'(Al_2CuMg)$	Laths	{210}
ν	Laths	{110}

The Al_3Zr phase is metastable to the extent that it precipitates during solution-treatment with an $L1_2$ structure and a spherical morphology. The metastable $L1_2$ Al_3Zr precipitate in aluminum-lithium alloys has been variously referred to as β' or α' (9,10). The α' designation was proposed by Gayle and Vardersande (10) to indicate that Li atoms substitute for Zr atoms in this $L1_2$ precipitate in Al-Li-Zr alloys. Frequently, when Al_3Zr and δ' (Al_3Li) occur in a system simultaneously, they coprecipitate, with δ' precipitating around Al_3Zr. Dark field imaging of this "composite" precipitate causes the Al_3Li to preferentially illuminate(10,11) providing the commonly observed "donut" morphology. In addition, it was also shown (10) that in Al-Li-Zr alloys, Al_3Zr has solubility for some Li at the solution treatment temperature and could retain Li atoms in supersaturation after quenching.

The δ' precipitate has an $L1_2$ structure with a very small lattice parameter mismatch with the matrix. It has a cube-on-cube orientation relationship with the matrix with $(111)\delta' \parallel (111)Al$. The $L1_2$ structure, in addition to the fcc spots, will exhibit the superlattice reflections such as (100) and (110). This is seen clearly in Figure 2 where the zone axis is [100]. Likewise, for B=[110], the δ' spots occur at the intersection of diagonals of a rhombus described by four adjacent matrix spots. When B=[112], the δ' spots line up as vertical rows midway between the matrix rows and lying on the same

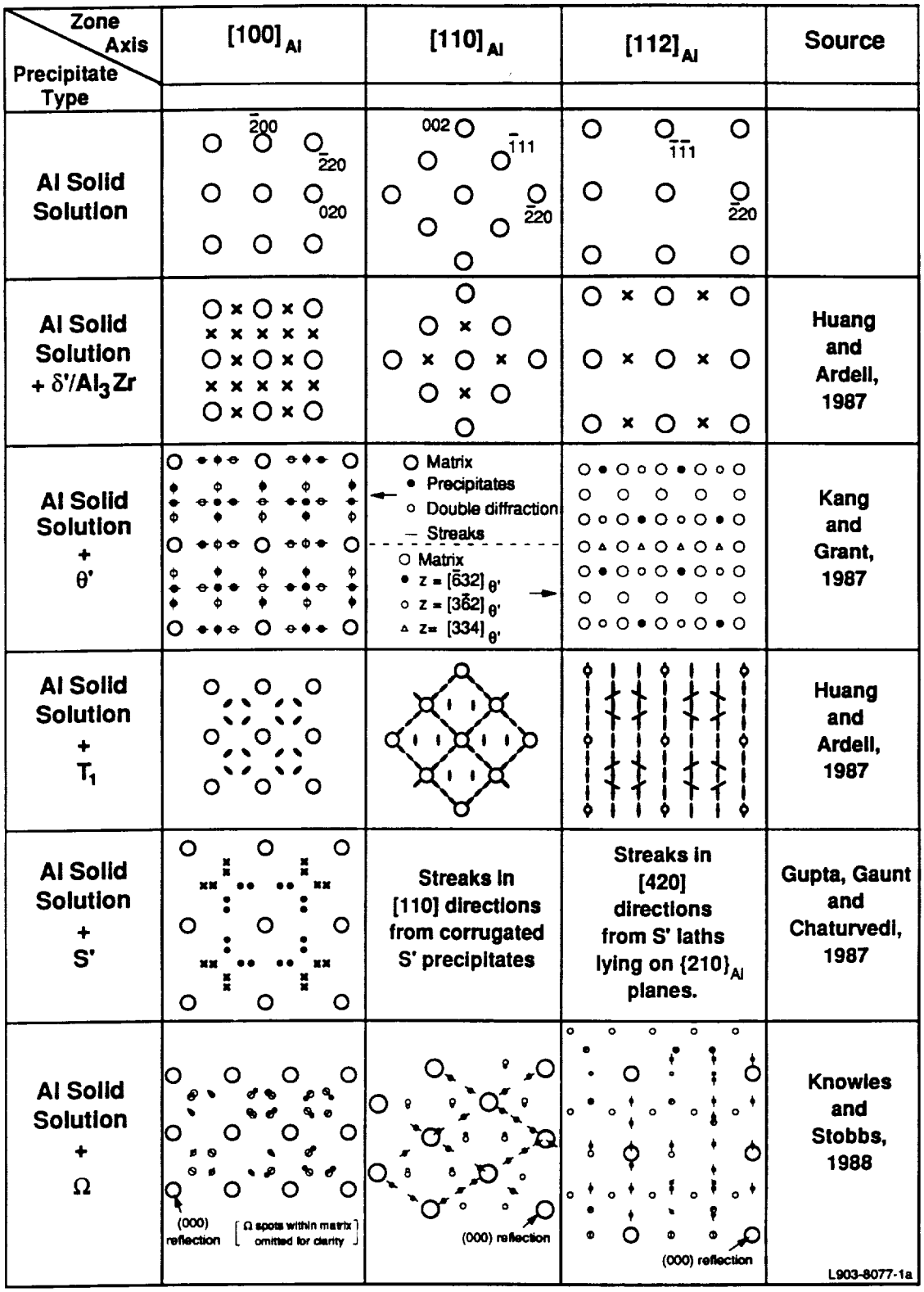

Figure 2 Schematic selected are diffraction patterns expected for the δ', θ', T_1 and S' phases in an aluminum solid solution matrix using the $[100]_{Al}$, $[110]_{Al}$ and $[112]_{Al}$ zone axes.

horizontal line as the matrix spots. It must be noted that Al_3Zr exhibits the same spot pattern as δ' and intensity effects are needed to discriminate between the two precipitates.

The θ' precipitates occur as disks lying on the {100} matrix planes. These are semi-coherent with the matrix. Since they lie on three orthogonal cube axis, for a [100] matrix zone axes, θ' manifests itself as vertical and horizontal streaks, for the two variants lying parallel to the beam direction with intensity maxima and double diffraction occurring as shown in Figure 2. The third variant lies normal to the beam direction and diffraction spots rather than streaks are generated that are coincident with the matrix and some of the δ' spots. For a [110] zone axis, θ' streaks are seen as the short diagonal of the rhombus described by four adjacent Al spots. Likewise, for a [112] matrix zone axis, the corresponding pattern due to θ' was generated by Kang and Grant (12) and is reproduced in Figure 2. Here the effect of double diffraction has not been included to retain clarity. In this case, the θ' spots lie in vertical columns midway between the columns of matrix spots and form horizontal rows of spots that alternate between matrix- and θ'-type. The GP1 zones and θ'' precursors to the θ' precipitates manifests themselves as more diffuse but continuous streaks in the <001> directions, with θ'' showing well defined intersection maxima at {100} matrix spots.

In Al-Cu-Li alloys, particularly 2090 and Weldalite™ 049*, the major strengthening phase is reported to be the T_1 phase. This phase has a hexagonal crystal structure with an orientation relationship of $(0001)T_1$ II {111}Al and $<1010>T_1$ II <110>Al (13,14). Huang and Ardell (15) have presented detailed experimental and theoretical evidence that shows that it was unnecessary to invoke the presence of the orthorhombic T_1' precursor proposed by Suzuki et al. (16) and by Rioja and Ludwiczak (17) to account for the extra diffraction spots that were observed. Subsequently, Cassada et al. (18) have independently confirmed the findings of Huang and Ardell (15).

*Lattice image work reported in the following section of this report addresses the exact nature of the "T_1-like" phase in Weldalite™ 049.

There are four variants of the T_1 phase and for an SAD pattern with a [100] matrix zone axis, these four variants produce four spots that are symmetrically distributed about the intersection of the diagonals of a square described by connecting the four adjacent matrix spots and lying on the diagonals (Figure 2). When the zone axis is matrix [110], then two variants of T_1 are inclined to the zone axis, and produce spots that lie along the long diagonal of the rhombus described by four adjacent matrix spots while the other two variants are parallel to the zone axis (the normal to the precipitate plane is normal to the zone axis) and produce streaks that form the sides of the rhombus just described. The electron diffraction pattern resulting from zone axis Z = [112] is shown in Figure 2. In this case, the four variants of T_1 produce spots and streaks. In this orientation, one variant of T_1 is normal to Z, the second is 19.5° from Z (i.e. angle included by Z and precipitate normal) and the third and fourth are 61.9° from Z. Thus, the first two variants are nearly parallel to the foil surface whereas the last two are fairly steeply inclined to it. Thus, in the diffraction pattern, spots, elongated spots and steaks are all seen making up the four variants. The two variants 61.9° away from Z produce similar elongated spots while the variant normal to Z produces the steaks.

The Ω phase (19), which is thought to be related to the equilibrium θ phase (Al_2Cu) and responsible for the unusually high strengths in non-lithium containing Al-Cu-Ag-Mg alloys, has an orthorhombic crystal structure (20-22) although, previously, Kerry & Scott (23) incorrectly ascribed a hexagonal structure to it based on SAD patterns. It was believed that the addition of trace amounts of Ag and Mg were together responsible for the formation of the Ω phase either directly or indirectly (22). Recently, however, a silver-free Al-Cu-Mg alloy was shown to contain small amounts of the Ω phase although adding trace amounts of Ag to it enhanced the amount of this phase (24). Two recent studies have attempted to identify the composition of the Ω phase (22,25) although there is no agreement in results.

A comparison of the SAD patterns for T_1 and Ω using [100], [110] and [112] matrix zone axis reveals only subtle differences that are difficult to discern when these precipitates are very thin due to streaking. In Al-Cu-Li-Ag-Mg alloys, as is the case in the present study, it becomes difficult to distinguish between the two if both indeed co-exist. It is conceivable that these two phases exhibit a mutual solid solution behavior and are indistinguishable from each

other. However, the high resolution work described in the next section indicates that Ω is not present in Weldalite™ 049 under the conditions investigated.

The orthorhombic S' phase(26) occurs in Al-Cu-Mg alloys and is the precursor to the equilibrium S phase (Al_2CuMg). When the Cu:Mg ratio is 2.2:1 then a pseudo-binary Al-Al_2CuMg system results (27,28). The S' phase nucleates on dislocation loops and helices formed during quenching (27) and grows as laths on {210} matrix planes along <100> matrix directions with the orientation relationship given by

$$[100]_{S'} \parallel [100]_{Al},\ [010]_{S'} \parallel [021]_{Al},\ [001]_{S'} \parallel [012]_{Al}$$

This precipitate matrix-orientation relationship gives rise to 12 possible orientation of S' laths in the Al matrix, four variants corresponding to each <100> matrix direction. Since these laths lie on {210} planes having a common <100> zone axis, they can form corrugated sheets of precipitate (27), lying on a (110) matrix plane (see Figure 11 of reference 27). According to another study (29), S' precipitated as rods with a diameter of ~90 Å rather than laths, and the observed difference in morphology was speculated to result from differences in the Cu:Mg ratio in the alloy. The small diameter was consistent with the streaking observed for the $(020)_{S'}$ and $(002)_{S'}$ reflection in the $[120]_{Al}$ and $[210]_{Al}$ directions. Long term aging did not cause these rods to coalesce to form laths; rather, there was some tendency for the rods to group together parallel to (110) and (110) and occasionally parallel to (100) and (010) matrix planes. A schematic diffraction pattern for the S' phase with a [001] matrix zone axis is shown in Figure 2. In addition, the S' phase can produce streaking in the $<210>_{Al}$ directions for $[100]_{Al}$ and $[112]_{Al}$ zone axis and in the $<110>_{Al}$ direction for a $[110]_{Al}$ zone axis. The observation of streaking in the $<110>_{Al}$ directions is rationalized on the basis of corrugated precipitate sheets lying on {110} matrix planes.

The role of the v phase (7) in affecting mechanical behavior remains to be established and whether it is indeed a new phase or a hitherto unreported variant of another phase such as S' remains to be confirmed.

3. EXPERIMENTAL PROCEDURE

An extrusion of an aluminum alloy, 9.5mm x 102mm in cross section, and of composition, 5.4Cu-1.64Li-0.4Ag-0.4Mg-0.16Zr (wt%), was solutionized at 493°C(766K) for 1h and water quenched to ambient temperature. A section of the extrusion was stretched 3% within 1h after quenching. The stretched and unstretched materials were allowed to naturally age at room temperature for >1000h to obtain the T3 and T4 conditions, respectively.

The artificial aging response was monitored using Rockwell B hardness measurements. The stretched material was aged at 160°C(433K) whereas the unstretched material was aged at 180°C(453K). Specimens were selected along the aging curves for microstructural examination in the transmission electron microscope (TEM).

Specimens for microstructural examination were sliced from the extrusions and mechanically ground to the desired thickness. These were then twin jet electropolished to perforation at -30°C(243K) and 12-15 volts in a solution of 25% HNO_3 in methanol. After polishing, the specimens were dipped in a solution of 50% HNO_3 in H_2O to remove any Ag which may have redeposited from the electrolyte. Bright field (BF), selected area diffraction (SAD) and centered dark field (CDF) imaging were used to follow the microstructural evolution during aging.

4. RESULTS AND DISCUSSION

4.1 Hardness Versus Aging Time

The unstretched material exhibits a stronger natural aging response compared to the stretched material, (R_B 80 vs R_B 68 after >1000h), Figure 1. Artificial aging was performed at 160°C(433K) for the stretched material and at 180°C(453K) for the unstretched condition. The open and full circles along the aging curves indicate the locations from where specimens were taken for microstructural analysis. In both instances, a reversion is observed with an appreciable decrease in hardness. This reversion is typically observed after approximately 15 minutes at temperature with the depth of the "reversion trough" being considerably greater for the unstretched material. Further aging causes an increase in hardness with a peak being observed, for both the stretched and unstretched material after

40-50h of artificial aging at the respective temperatures. For longer times at each aging temperature (~200h), the hardness decrease is minimal, Figure 1.

The observed reversion trough is of technological relevance because at the bottom of the reversion trough, the material is in a lower-strength, high-ductility condition, i.e. 24% typical elongation (1) -- one that provides the potential for near-net shape cold forming after solution heat treatment and quenching thereby eliminating the distortion that would accompany a subsequent quench. Gayle, et al. (6) have shown that in Weldalite™ 049, (i.e., a similar alloy but with 1.3 wt%Li), room temperature re-aging of the unstretched material following a reversion treatment returned the strength to the original T4 level after an extended incubation period. The incubation time can be about 5 days before hardness increases again and this allows sufficient time for a part to be formed.

4.2 Microstructure of the Naturally-Aged Material

The microstructure of the naturally aged unstretched material (T4) was examined using TEM and an SAD pattern corresponding to the $[100]_{Al}$ zone axis (Figure 3a) reveals streaking associated with GP zone formation and superlattice reflections characteristic of δ'. The GP zones lie on $\{100\}_{Al}$ planes, are fine and appear fairly well developed compared to other Cu-containing aluminum alloys. The δ' precipitates are also extremely fine and evenly distributed throughout the matrix, except for the situation where they precipitate around the previously existing Al_3Zr to form the "composite" precipitates. These observations are consistent with earlier reports on the natural aging response of the 1.3 wt.% Li content alloy, Weldalite™ 049.

In the stretched, naturally aged material, (T3), streaking due to well developed GP zones observed for the T4 condition is not seen and only δ' reflections are evident, Figure 3b. Apparently the stretching operation discourages GP zone formation. The volume fraction and size of the δ' precipitation relative to the unstretched material is approximately the same as observed from dark field studies. A similar response was also observed in the alloy containing 1.3 wt.% Li (5).

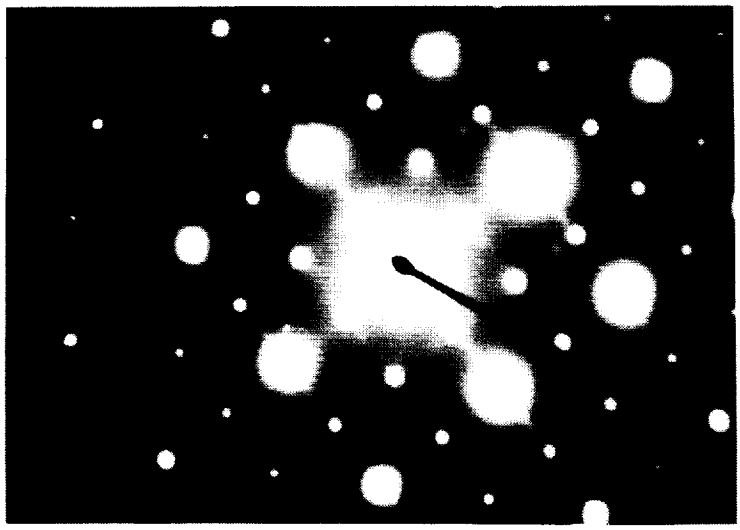

(a)

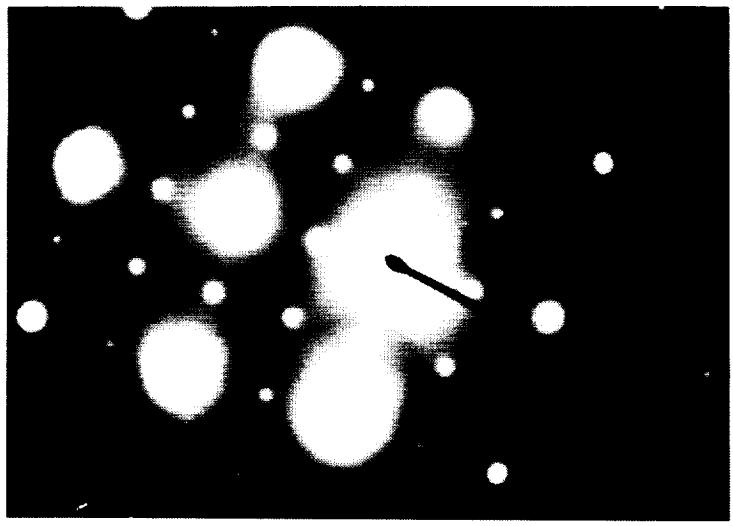

(b)

Figure 3 SAD patterns obtained using $[100]_{Al}$ zone axis for the naturally aged material (a) previously unstretched and (b) with 3% prior stretch.

4.3 Microstructure of the Artificially Aged Unstretched Material

Although the hardness-versus-aging time profile for the unstretched material was generated at 180°C(453K), specimens were heat treated at 160°C(433K) also for 15 minutes to provide a direct comparison of the reversion behavior with the stretched material. A diffraction pattern with a $[112]_{Al}$ zone axis of a specimen heat treated for 15 minutes at 160°C(433K) reveals the presence of δ' (Figure 4a). A similar heat-treatment at 180°C(453K) however, causes all the δ' to dissolve as evidenced by the absence of superlattice reflections in the SAD pattern in Figure 4b, taken using a $[100]_{Al}$ zone axis. In both instances, the GP zones were not longer seen. These observations are different from those reported by Gayle et al. (6,7) on the lower Li-containing Weldalite™ alloy. When the thin foil specimen used to obtain Figure 4b was examined two weeks later, room temperature aging had caused the δ' to reprecipitate as can be seen from the superlattice spots in Figure 4c. This natural aging response of the reverted material is consistent with earlier observations and may have technological significance as discussed earlier.

Aging the unstretched material at 180°C(453K) for longer times causes the hardness to increase and after 2h, the hardness is approximately equal to that in the naturally aged condition (Figure 1). A thin foil specimen oriented with a $[110]_{Al}$ zone axis (Figure 5a) reveals the presence of faint spots characteristic of the T_1 variants, δ', superlattice spots and streaking in the $[100]_{Al}$ direction, indicating the presence of the θ' phase. It is interesting to note that the T_1 with its four variants should exhibit streaking in the [111] directions in addition to the two spot variants but these streaks are not obvious in this heat-treated condition. A dark field image of the δ' precipitates using the corresponding superlattice reflection in Figure 5a is shown in Figure 5b. The δ' precipitates are seen either as halos around the Al_3Zr precipitates or forming independently. At this stage, these δ' precipitates are ~100Å in size. The Al_3Zr precipitates tend to be larger (~250-300Å). As the [100] streak corresponding to θ' (Figure 5a) passes through the δ' superlattice spot, dark field imaging of δ' will include information characteristic of θ'. A bright field-dark field pair in figures 5c and 5d show the precipitation of fine, thin T_1 platelets, primarily on the sub-boundaries. These platelets are approximately 600 Å in length. Clearly T_1 precipitation commences on the sub

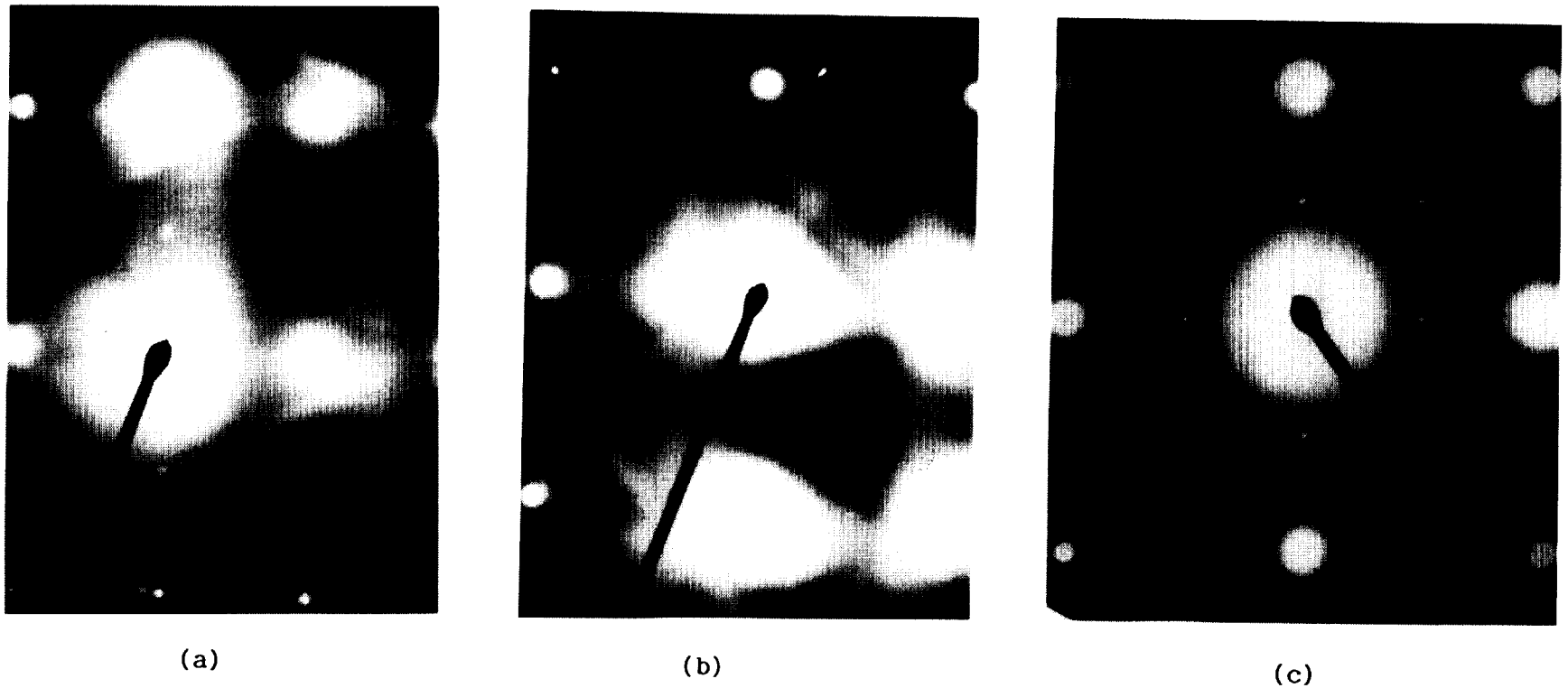

(a) (b) (c)

Figure 4 Diffraction patterns from unstretched material: (a) $[112]_{Al}$ zone axis of a specimen heat-treated for 15 minutes at 433K, (b) $[100]_{Al}$ zone axis of a specimen heat-treated for 15 minutes at 453K and (c) $[100]_{Al}$ zone axis of a specimen aged as in (b) and then subsequently naturally aged for two weeks at room temperature.

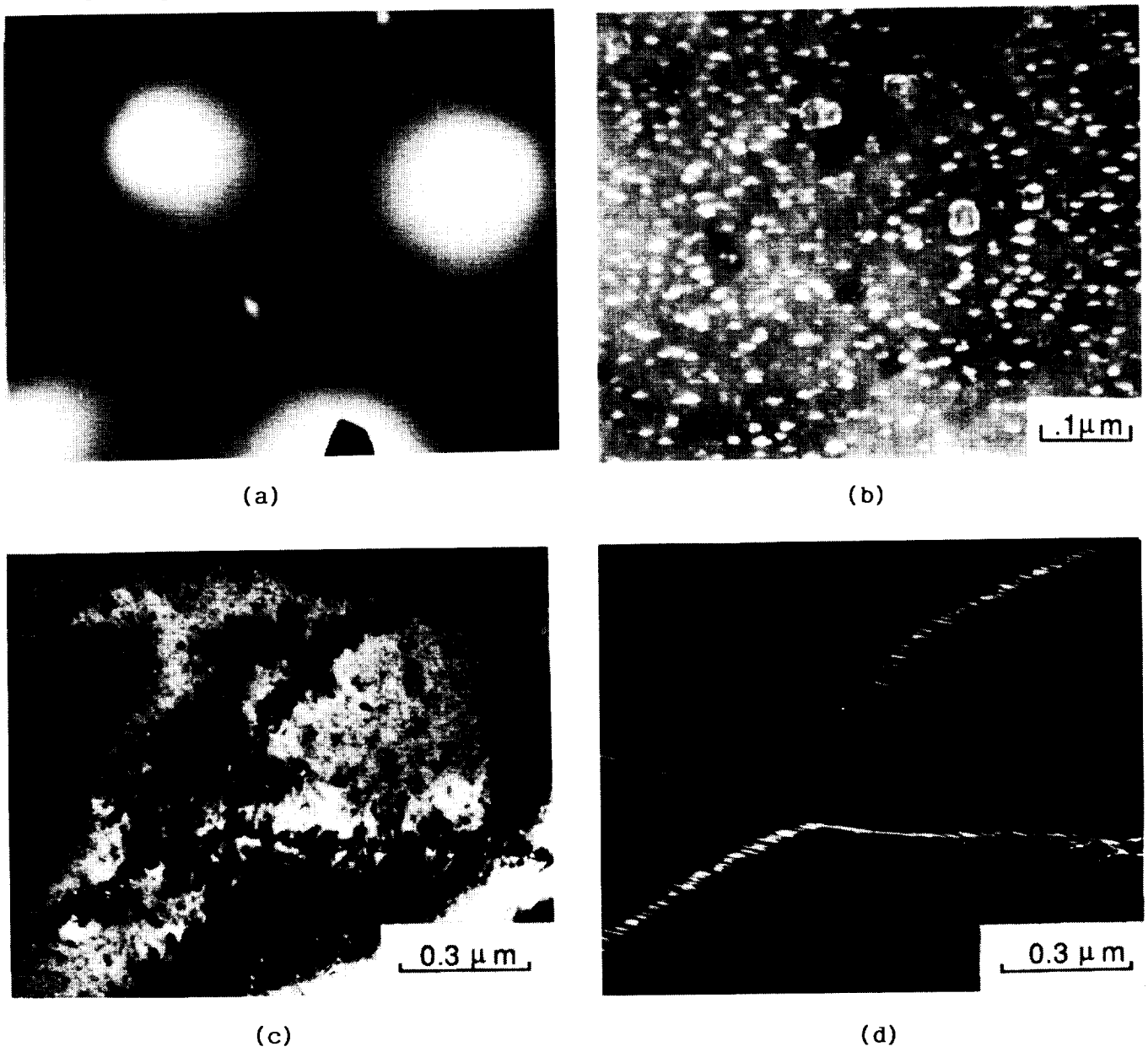

Figure 5 An unstretched specimen heat treated for 2h at 453K: (a) $[110]_{Al}$ zone axis SAD pattern, (b) δ' dark field micrograph, (c) general bright field showing sub-boundaries and (d) T_1 dark field showing preferential precipitation of T_1 at sub-boundaries seen in (c).

boundaries during these early stages of aging, with the loosely knit walls of dislocations serving as preferential nucleation sites.

Aging the unstretched material for even longer times (for 6h at 180°C causes further precipitation of T_1 as can be seen in the bright field image in figure 6a. At least three of the four T_1 variants are readily seen with fringe contrast from the extremely thin T_1 platelets being observed for two variants. The third variant is seen with an edge-on orientation. These precipitates appear to be distributed in the matrix, in contrast to those observed at the earlier aging time of 2h at 180°C(453K) where the T_1 precipitates were observed primarily at the sub-boundaries (Figure 5d). A diffraction pattern obtained using the $[110]_{Al}$ zone axis reveals the presence of a wealth of precipitates. The four variants of the T_1 phase manifest themselves as two sets of streaks and two sets of spots. The streaks correspond to the edge-on orientation and describe a rhombus in Figure 6b. The two sets of spots lie on the long diagonal of this rhombus at one third and two thirds of this diagonal (see Figure 6b and compare with Figure 2). In addition, faint streaking is also observed along this long diagonal which corresponds to the $[110]_{Al}$ orientation and suggests the presence of precipitates on the $(110)_{Al}$ planes. This likely occurs from the S' precipitates that have $\{210\}_{Al}$ habit planes and form a corrugated sheet that lie on the (110) matrix planes. Streaking is also observed in the $[100]_{Al}$ orientation corresponding to the short diagonal of the rhombus and indicative of the presence of θ' precipitates with $[100]_{Al}$ habit planes. A bright spot is also observed at the intersection of the long and short diagonals of the rhombus. This can simply be an intersection maximum or, alternately, it can correspond to a δ' superlattice reflection. In this case dark-field imaging was used to confirm the presence of δ' precipitates. Dark field imaging of one of the four T_1 variants using one of the two spots in Figure 6b shows the fine T_1 platelets in Figure 6c. The edge-on variant at the sub-boundaries and in the matrix is shown in figure 6d and at this stage of aging T_1 has precipitated within the matrix causing a sub-boundary precipitate free zone.

After 12h at 180°C(453K), a still substantially underaged condition based on hardness variation with aging time (Figure 1), the microstructure consists of T_1, θ', S', and δ'. The presence of these phases can be verified in Figure 7a which shows a diffraction pattern obtained using a $[110]_{Al}$ and $[100]_{Al}$ orientations (long and short

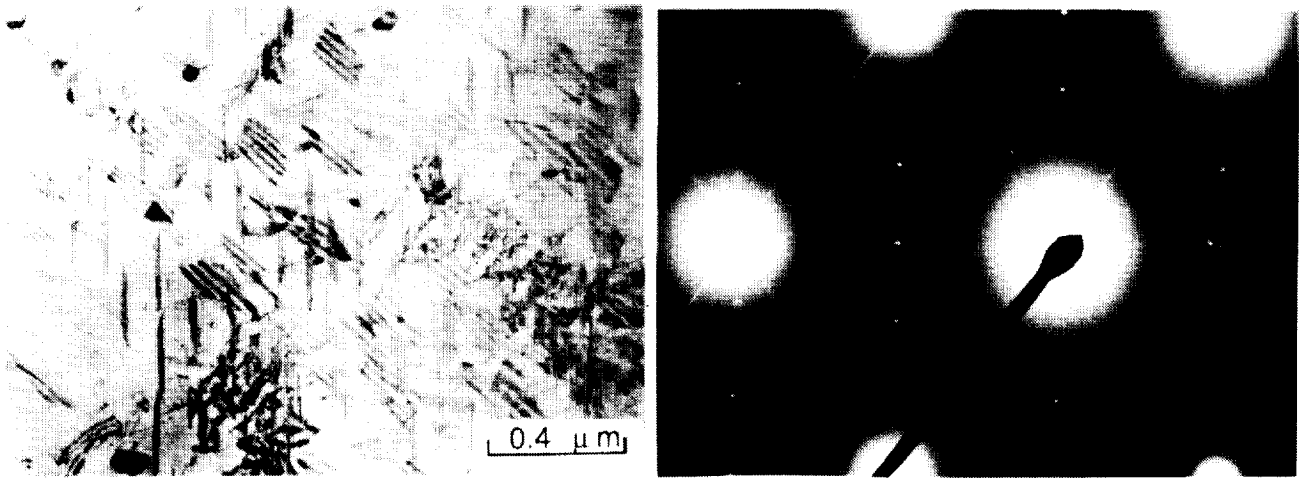

(a) (b)

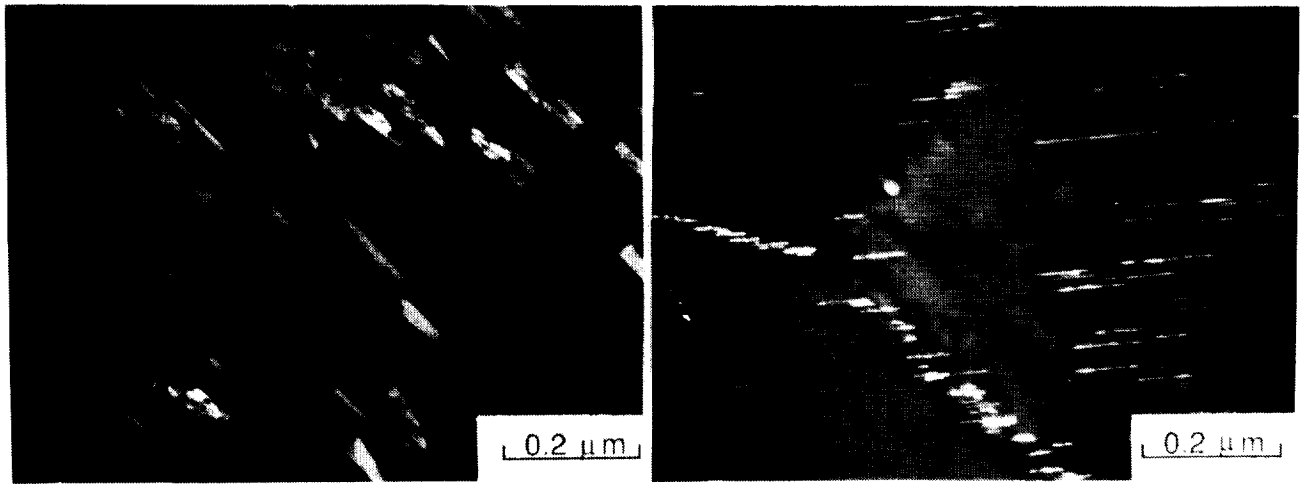

(c) (d)

Figure 6 Microstructure of the unstretched material aged for 6h at 453K showing (a) variants of T_1 using bright field, (b) SAD pattern with $[110]_{Al}$ zone axis confirming T_1, δ', θ' and S', (c) dark field of one of the T_1 variants and (d) dark field of T_1 precipitation in the interior of subgrains and at sub-boundaries.

diagonals respectively of the rhombus described using four adjacent matrix spots) confirms the presence of S' and θ' while the bright spot at the intersection of the two streaks verifies the existence of δ'. A bright field image (Figure 7b) located adjacent to a sub boundary reveals the presence of T_1, in the matrix, at the sub-boundaries and in the regions which previously appeared to be precipitate free zones (Figure 6d). Thus, it appears that in the unstretched material, T_1 precipitation commences at the sub-boundaries, then occurs within the subgrains, creating a subgrain precipitate free-zone which fills out fairly homogeneously with further aging. This whole sequence occurs within the first 12h of artificial aging, which still lies well within the underaged regime (R_B = 83), since near-peak aging requires ~34h at 180°C (R_B = 88).

A bright field reference, the associated SAD pattern taken with a $[110]_{Al}$ zone axis and dark field images of δ', θ', one variant of T_1 and S' are shown in Figures 8a-f. The SAD pattern in Figure 8b reveals the four T_1 variants, δ', streaking in the [110] orientation associated with S' and streaking in the [100] direction associated with θ'. The SAD pattern was intentionally oriented so as to maximize θ' and S' streak intensities. A dark field image of the δ' precipitates reveals some unusual features, Figure 8c. These δ' precipitates are ellipsoidal in shape rather than spherical and appear to have a thin line of extinction running along the major axis of the ellipse (see inset in Figure 8b). If this figure is superimposed on Figure 8c, which is a dark field image of θ', it is found that the θ' precipitates fit quite well along the major axis of several of the δ' precipitates in Figure 8b suggesting δ' precipitation on θ'. The S' precipitates (Figure 8f) appear to be fairly uniformly distributed in this unstretched material which is unusual considering a recent study (30) on Al-Li-Cu-Mg alloys that shows that the stretching operation prior to aging is essential to obtain a uniform distribution of the S' phase.

A region adjacent to sub-boundaries after 12h aging at 180°C(453K) (Figure 9a) reaveals that the sub-boundaries contain the T_1 phase as does the matrix. In addition to the two-edge-on variants of T_1 in Figure 9a, two additional edge-on variants are visible almost parallel and perpendicular to the sides of the figure, and are thought to correspond to S'. A dark field image of δ' in Figure 9b reveals δ' precipitation around Al_3Zr. The region corresponding to the far right

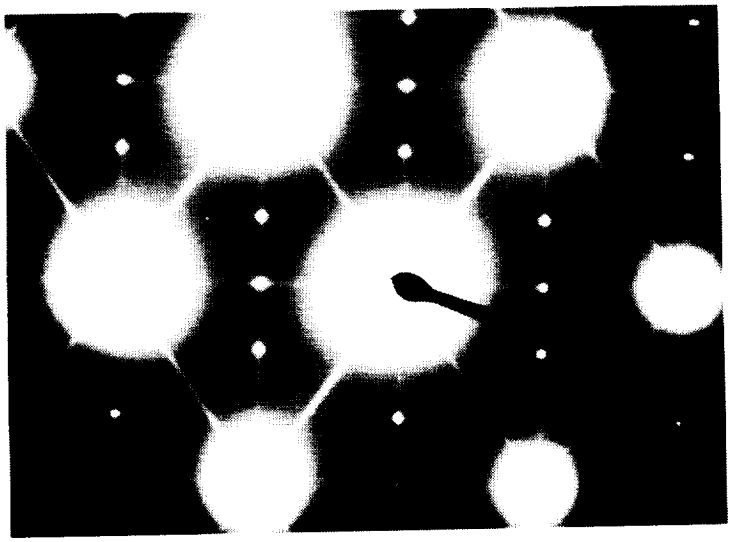

(a)

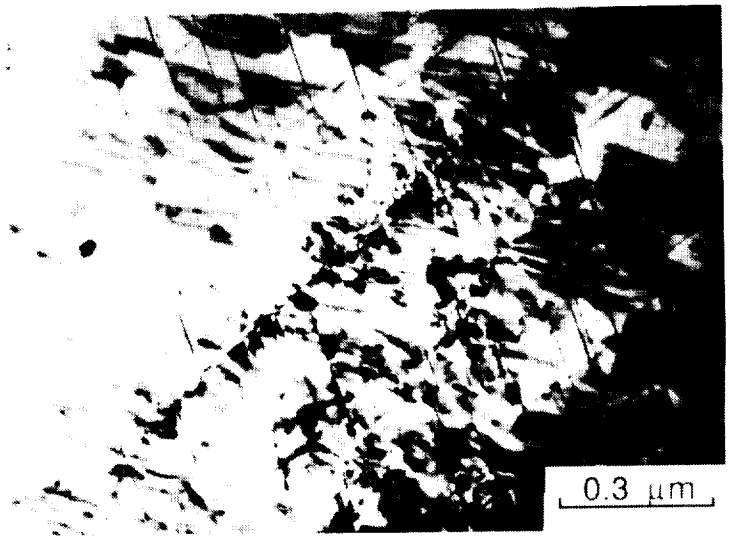

(b)

Figure 7 An unstretched specimen aged for 12h at 453K reveals (a) the presence of T_1, δ', θ' and S' in a $[110]_{Al}$ zone axis SAD pattern and (b) a homogeneous distribution of T_1 at sub-boundaries, interior of sub-grains and in the regions adjacent to the sub-boundaries.

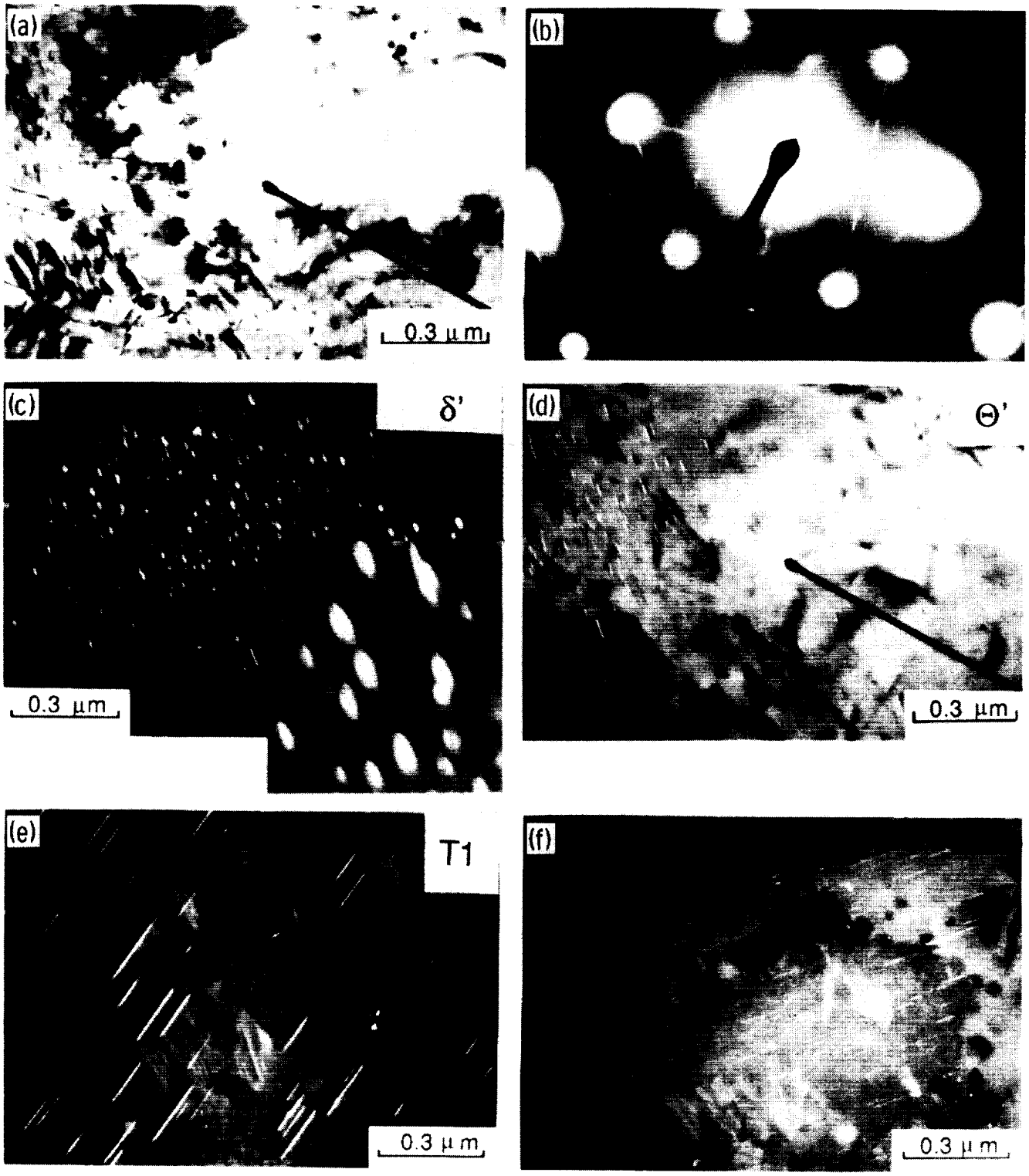

Figure 8 Microstructure of an unstretched specimen aged 12h at 453K using (a) reference bright field image, (b) associated SAD pattern, (c) δ' dark field, (d) θ' dark field, (e) T_1 dark field and (f) S' dark field.

ORIGINAL PAGE
BLACK AND WHITE PHOTOGRAPH

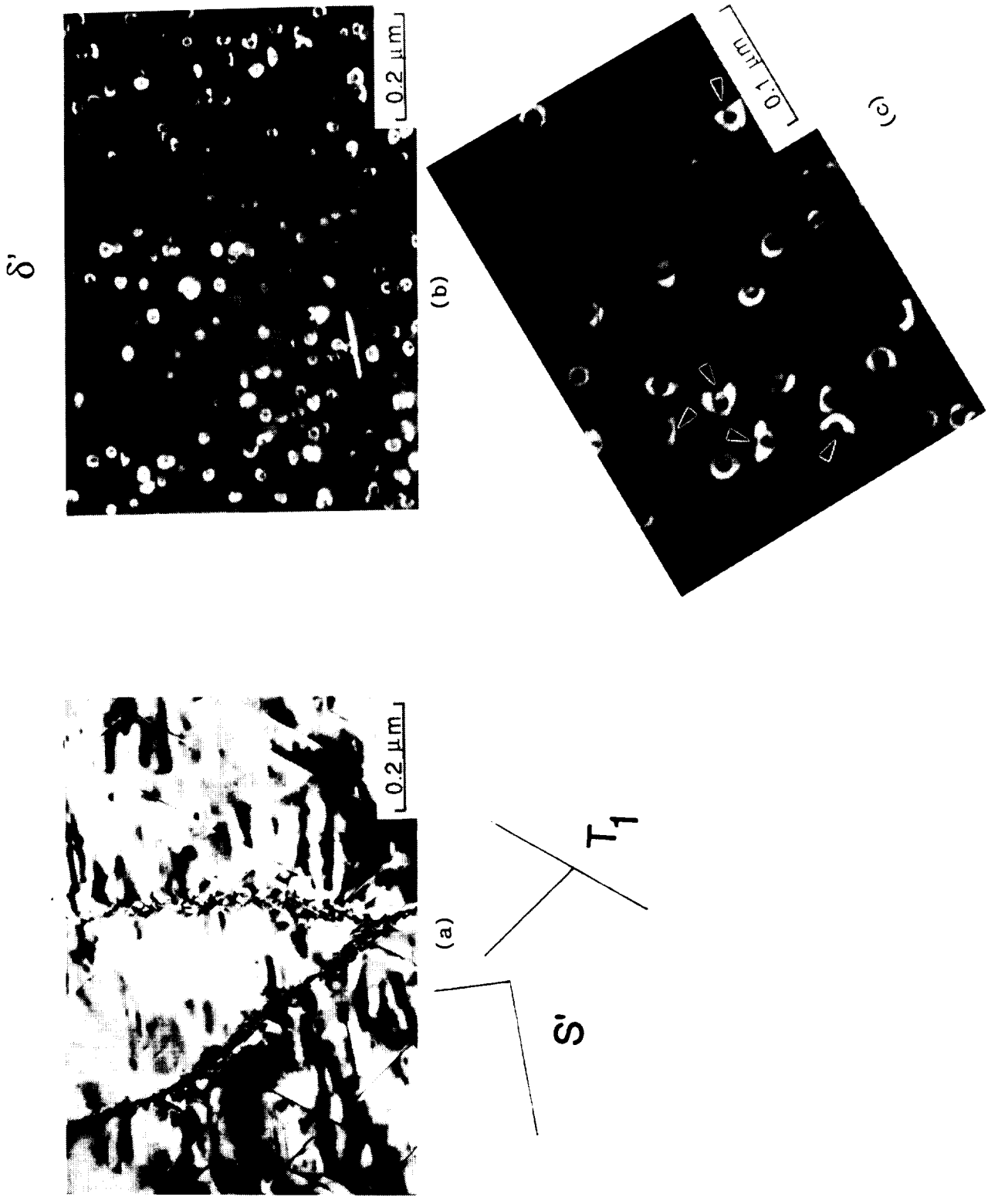

section of Figure 9b is shown at a higher magnification in Figure 9c, after accounting for the rotation involved due to changes in magnification in the TEM. From the two dark field micrographs, Figures 9b and 9c, it is seen that the δ' precipitates do not form a complete "halo" around Al_3Zr; rather in several instances they end abruptly forming a cross section contained by a chord of a circle on that side. Several such instances are indicated in Figure 9c. A comparison of the orientation of the "chords" in Figure 9c with Figure 9a reveals them to be frequently coincident with the orientation of the S' precipitates although occasionally they also are parallel to T_1 edge-on variants. This may suggest the heterogeneous precipitation of T_1 and S' at the $Al_3Zr/Al_3Li/\alpha$-matrix interfaces. It is possible that the precipitation of Al_3Li causes a local enrichment of Cu and Mg, allowing the formation of S' and to a lesser extent T_1 at these interfaces.

Overaging the unstretched material for 48h at 180°C(453K) results in a significant decrease in intensity of the δ' superlattice spots (Figure 10a) located at the center of each rhombus described by joining four adjacent matrix spots in an SAD pattern generated using a [110]m zone axis. An enlargement of a portion of the SAD pattern is also shown in Figure 10a to emphasize this observation. All four variants of T_1 are present and, in addition, streaking due to θ' and S' are still visible. The [420] streaks in Figure 10b arising from S' with {210} habit planes are also clearly seen. Further, the [100] streaks due to θ' in Figure 10a and the θ' streaks and spots in the SAD pattern in Figure 10c generated using a $[100]_{Al}$ zone axis, are weaker relative to the T_1 streaks and spots, suggesting some dissolution of θ'.

Further over-aging for 100h at 180°C(453K) causes only a negligible decrease in hardness (Figure 1) and the associated microstructure is shown in Figure 11a as a bright field image. Both, a grain boundary and a sub boundary can be seen and a small grain boundary precipitate free zone is present whereas this is not the case for the sub boundary. Additionally, coarse (~0.1μm) grain boundary precipitates are seen and based on their size, it is not clear whether they were present prior to aging or occurred during aging. An enlarged portion of an SAD pattern, obtained using a $[110]_m$ zone axis is shown in Figure 11b. This Figure shows the region bound by four adjacent matrix spots and it is seen that the T_1 phase predominates with a faint δ' spot being present in the center of the rhombus. Streaking in the [420] orientation in Figure 11c, obtained using a $[112]_{Al}$ zone axis

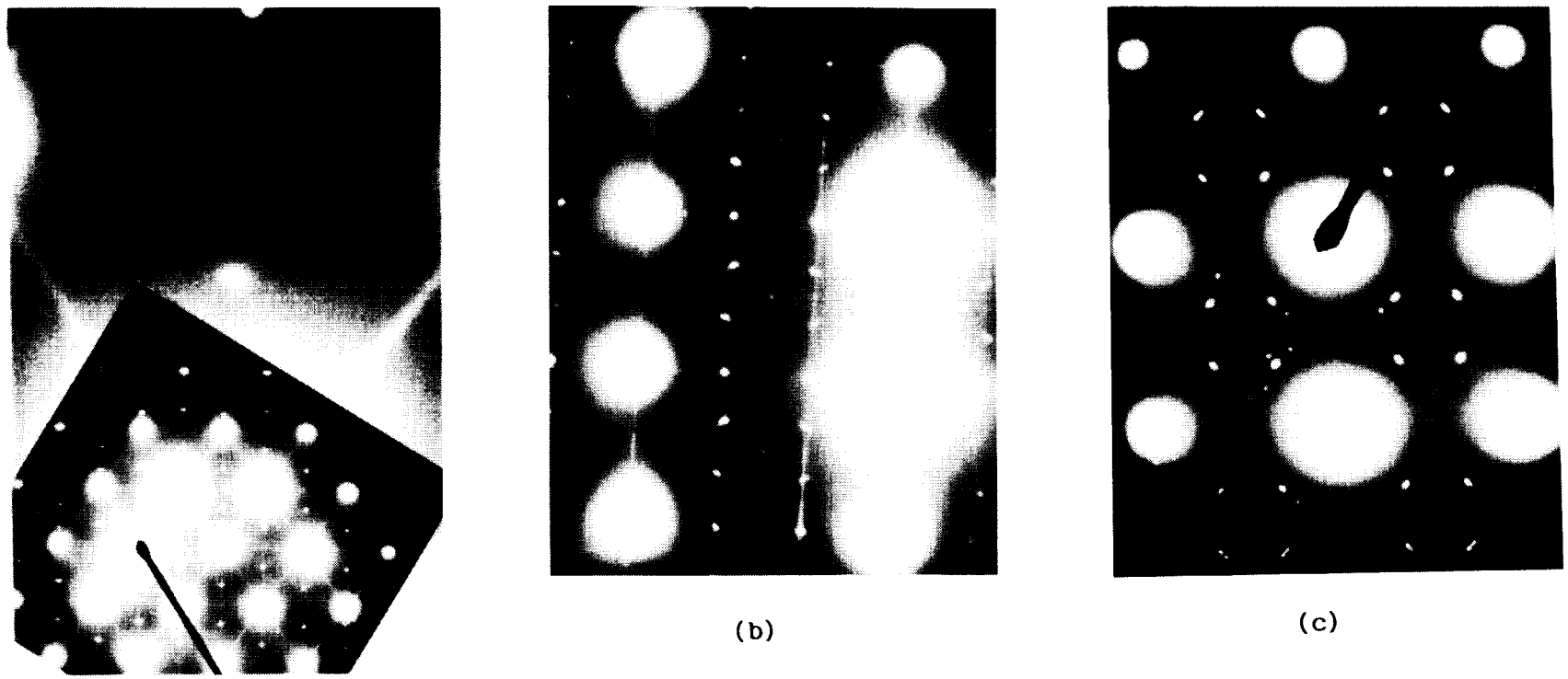

Figure 10 Selected Area Diffraction patterns obtained from an unstretched specimen-aged for 48h at 453K using (a) $[110]_{Al}$ zone axis, zone axis, (b) $[112]_{Al}$ zone axis and (c) $[100]_{Al}$ zone axis.

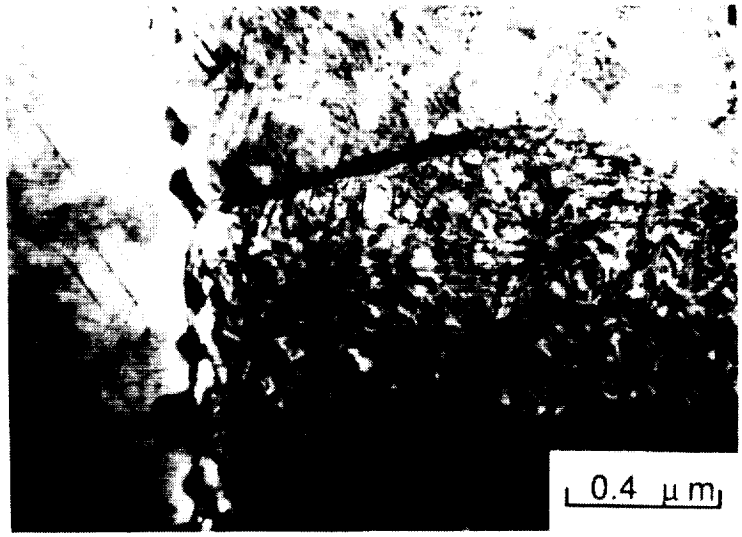

(a)

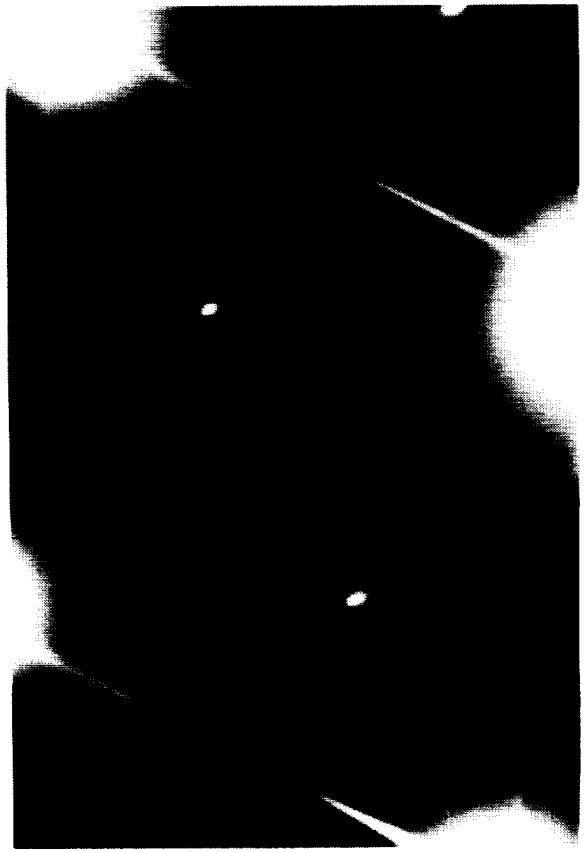

(b)

(c)

Figure 11 Overaged microstructure (100h at 453K) of an unstretched specimen revealing (a) sub-boundary and grain boundary precipitation in bright field (b) the absence of θ' streak and faint δ' spot in an SAD pattern with $[110]_{Al}$ zone axis and (c) presence of [420] S' streaks in an SAD pattern obtained using $[112]_m$ zone axis.

confirms the existence of the S' phase. If θ' is present it is only in very small amounts, as any streaking in the [100] orientation is extremely weak in intensity.

In summary, for the unstretched material, naturally aged strength results from fine δ', GP zones, and probably solid solution strengthening. Upon artificial aging at 180°C(453K), the GP zones dissolve as do some of the δ' precipitates causing a reversion associated with a decrease in hardness. Additional exposure to the artificial aging temperature results in the precipitation of T_1, initially at sub-boundaries, then in the interior of the subgrains. In addition, S', θ' and more δ' precipitate. Extensive over-aging appears to cause δ' and θ' to redissolve leaving predominantly T_1, and some S' precipitates, in the matrix.

4.4 Microstructure of the Artificially-Aged Stretched Material

It was shown in Figure 3b that natural aging of the stretched material results in strengthening predominantly from δ'; the formation of GP zones appears to be inhibited by the prior stretch.

Upon artificially aging the naturally aged material at 160°C(433K) for ~15 minutes, a decrease in hardness is observed (Figure 1) due to a reversion phenomenon. The decrease in hardness however, is not as large as was observed for the unstretched material; further, the hardness of the reverted material is higher than that of the unstretched material, similarly heat treated for 15 minutes, although at the higher temperature of 180°C(453K). A diffraction pattern of the stretched and reverted material, using a $[110]_{Al}$ zone axis, Figure 12a reveals the complete dissolution of the δ' precipitates as evidenced by the absence of the superlattice reflections indicative of δ'. Natural aging of the reverted material for a period of two weeks, causes the reprecipitation of δ', Figure 12b, likely restoring most, if not all of the hardness of the naturally aged material, prior to the reversion treatment.

While a 15 minutes exposure to 160°C(433K) causes essentially the complete dissolution of δ', leading to the observed reversion behavior, longer exposures to this temperature leads to the precipitation of some θ' and reprecipitation of δ', as is observed after

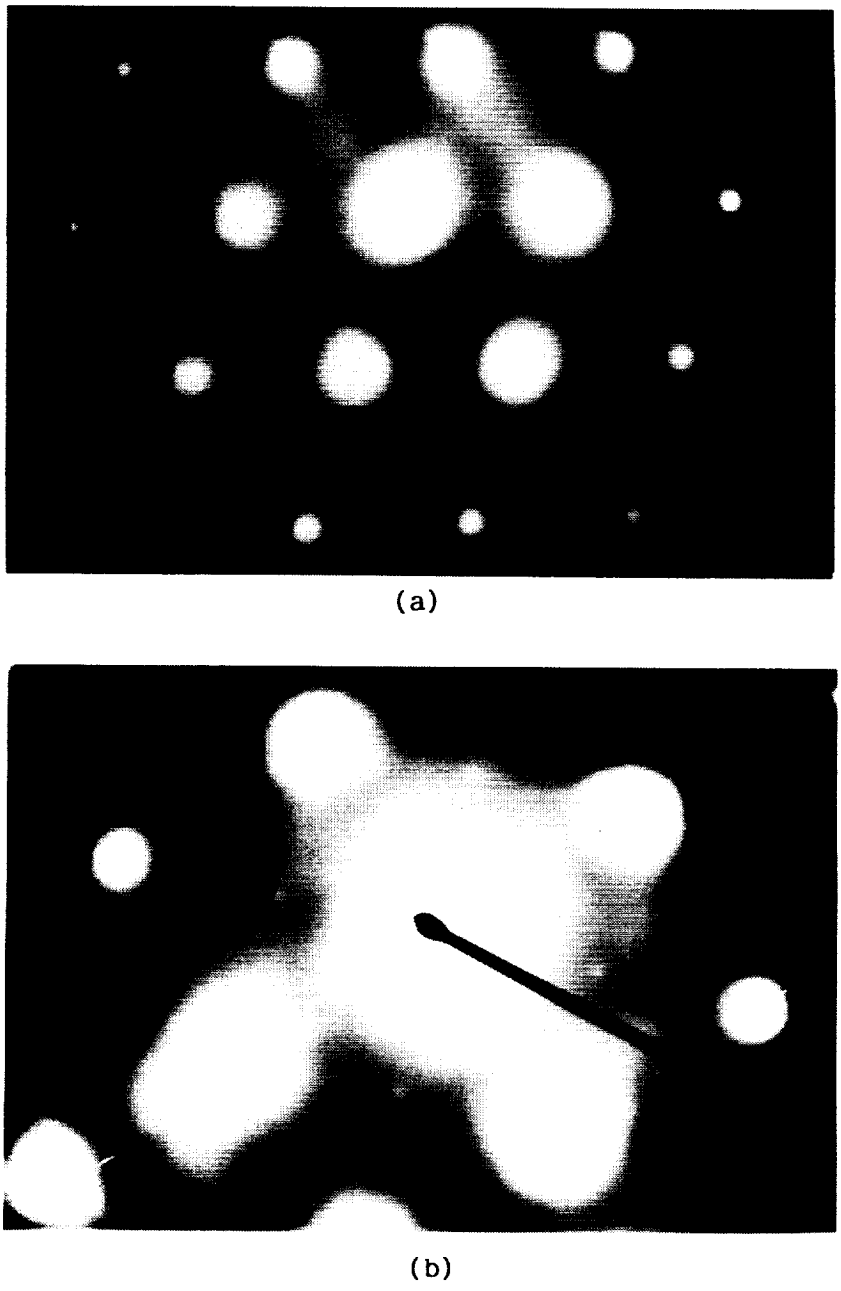

Figure 12 Diffraction patterns form the stretched material: (a) $[110]_{Al}$ zone axis of a specimen heat-treated for 15 minutes at 433K and (b) $[100]_{Al}$ zone axis of specimens in (a), subsequently naturally aged for two weeks at room temperature.

2h at 160°C(433K) (Figure 13a). After 6h at 160°C(433K), the δ' diffraction spots are much stronger (Figure 13b), and in addition, streaking is observed in the $[100]_{Al}$ directions, which is indicative of θ'. The four variants of the T_1 phase manifest themselves as 4 spots, positioned symmetrically around the δ' spots in Figure 13b, obtained using a $[100]_{Al}$ zone axis. At this stage, the intensity of the T_1 spots is weak relative to the δ' spots. A $[112]_{Al}$ zone axis SAD pattern in Figure 13c reveals the presence of streaks in the <420> directions indicative of the presence of the S' phase. The hardness of the stretched material after 6h at 160°C(433K) is R_B 78, which is similar to the hardness of the naturally-aged unstretched material, although the phases responsible for providing these similar levels of strength in two cases are different; in the naturally aged material, it was a combination of GP zones and δ', in this artificially aged condition it is a mixture of δ', θ', S' and T_1. The intensity of the T_1 spots increases significantly with a longer aging time of 10h at 160°C(433K) as can be seen by comparing Figure 13d with Figure 13c, although the θ' streaks in the $[100]_{Al}$ directions continue to remain weak. In the peak-aged condition of 34h at 160°C(433K), T_1, δ' and θ' were observed using a $[100]_{Al}$ zone axis to obtain the SAD pattern in Figure 14a. The intensities of the θ' spots and [100] streaks were weak and this behavior was also observed using a $[100]_{Al}$ zone axis. Thus the θ', spots and streaks remain weak for the stretched material in all the specimens examined after aging for various times at (433K).

Over-aging, i.e. 240h at 160°C(433K) causes additionally a decrease in the intensity of δ' spots, leaving behind only T_1 spots and streaks, as seen in the SAD pattern in Figure 14b obtained using a $[100]_{Al}$ zone axis. The presence of S' was confirmed using a $[112]_{Al}$ zone axis SAD pattern. Thus in the overaged condition, θ' could not be detected and intensity from δ' spots had decreased significantly compared to the peak-aged condition leaving behind some δ', predominantly T_1, and additionally, the S' phase.

In summary, stretching prior to aging appears to discourage GP zone formation in the naturally aged material, thereby causing the natural aging response to be less dramatic relative to the unstretched material. Upon artificial aging at 160°C(433K), reversion occurs, associated with the dissolution of δ'. Longer aging times at temperature results in the precipitation of T_1, S', and θ' and the

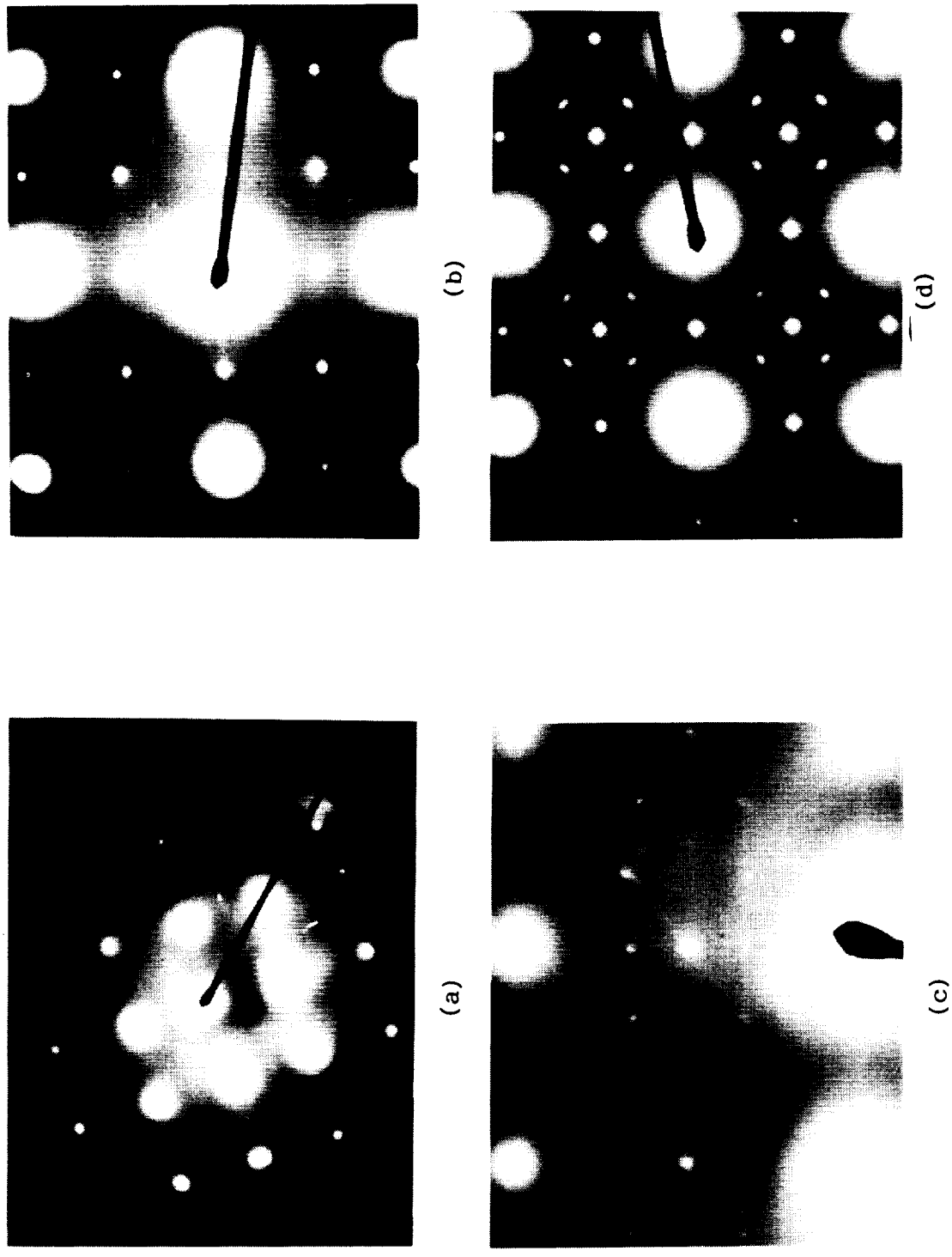

Figure 13 Selected are diffraction patterns from specimens aged for various time at 433K: (a) $[100]_{Al}$ zone axis from a specimen aged for 2h, (b) $[100]_{Al}$ zone axis and (c) $[112]_{Al}$ zone axis from a specimen aged for 6h and (d) $[100]_{Al}$ zone axis for a specimen aged for 10h.

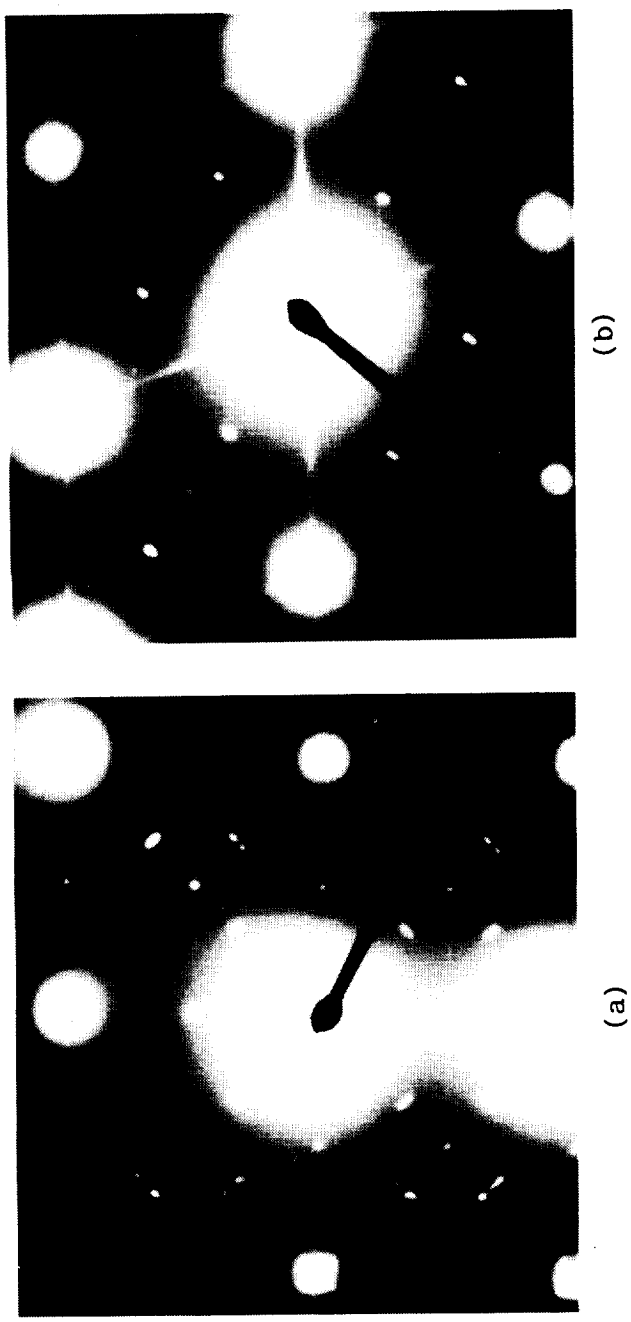

Figure 14 Stretched specimens aged for (a) 34h at (433K), $[100]_{Al}$ zone axis and (b) 240h at 433K, $[110]_{Al}$ zone axis.

reprecipitation of δ'. The intensity of spots and streaks related to θ' remain weak up to the peak-aged condition signifying that the prior stretch discourages θ' formation. This is unusual in high Cu-containing Al alloys and possibly arises from competitive nucleation and growth between T_1 and θ'; in this instance it appears that T_1 is the favored phase. In the overaged condition θ' was not detected and the intensity of δ' spots is low suggesting redissolution of δ', possibly related to the dissolution of θ'. Finally, the phases found at the various stages of aging after stretching are compared with those found without stretch in Table 15.

Table 15. Summary of Phases Present and Diffraction Information in Higher Li-Containing Weldalite™ Alloy

(Al-5.35Cu-1.64Li-0.40Ag-0.44Mg-0.16Zr, wt%)

Aging Time	Unstretched 180°C (aging temperature)	Stretched 3% 160°C (aging temperature)
0 (i.e. T4, T3)	δ', GP Zones	δ' + weak GP Zones
+ 1/4 h	weak δ'	weak δ'
+ 2 h	δ', θ', T_1, <110> streaks	δ', T_1?
+ 6 h	δ', θ', T_1, <110> streaks	δ', T_1, weak θ', weak <110>, S'
+ 10 h	-	δ', T_1, θ', <110>, S'
+ 12 h	δ', T_1, θ', <110> streaks, S'	-
+ 34 h	-	δ', T_1, θ', S'
+ 48 h	weak δ', T_1, θ', <110> streaks, S'	-
+ 100 h	weak δ', T_1, weak θ', <110> streaks, S'	-
+ 240 h	-	δ', T_1, S' [θ', not seen]

5. REFERENCES

[1] J.R. Pickens, F.H. Heubaum, T.J. Langan and L.S. Kramer in "Aluminum-Lithium Alloys" (Proceedings of the Fifth International Aluminum-Lithium Conference), eds: T.H. Sanders and E.A. Starke, MCE Publication Ltd., Birmingham, U.K., 1989, p. 1397.

[2] R.J. Rioja, P.E. Bretz, R.R. Sawtell, W.H. Hunt and E.A. Ludwiczak, in "Aluminum Alloys, Their Physical and Mechanical Properties," Vol. III, Proceedings of the International Conference on Aluminum Alloys, Chameleon Press, London, U.K., 1986, p. 1781.

[3] W.A. Cassada, G.J. Shiflet and E.A. Starke, Jr., J. de Physique, Colloq. C3, Vol. 48, 1987, p. 397.

[4] T.J. Langan and J.R. Pickens in "Aluminum-Lithium Alloys" (Proceedings of the Fifth International Aluminum-Lithium Conference), eds: T.H. Sanders and E.A. Starke, MCE Publication Ltd., Birmingham, U.K., 1989, p. 691.

[5] K.S. Kumar, S.A. Brown and J.R. Pickens, Scripta Metall. et Mater., 24, 1990, p. 1245.

[6] F.W. Gayle, F.H. Heubaum and J.R. Pickens in "Aluminum-Lithium Alloys" (Proceedings of the Fifth International Aluminum-Lithium Conference), eds: T.H. Sanders and E.A. Starke, MCE Publications Ltd., Birmingham, U.K., 1989, p. 701.

[7] F.W. Gayle, F.H. Heubaum and J.R. Pickens, Scripta Metall., 24, 1990, p. 79.

[8] J.R. Pickens, F.H. Heubaum, T.J. Langan, and L.S. Kramer, in "Aluminum-Lithium Alloys" (Proceedings of the Fifth International Aluminum-Lithium Conference), T.H. Sanders and E.A. Starke, eds., MCE Publications Ltd., Birmingham, U.K., 1989, p. 1397.

[9] P.L. Makin and B. Ralph, J. Mater. Sci., 19, 1984, p. 3835.

[10] F.W. Gayle and B. VanderSande, Acta Metall., 37, 1989, p. 1033.

[11] P.L. Makin, D.J. Lloyd and W.M. Stobbs, Philos. Mag. Letters, Philos. Mag. A, Vol. 51, #5, 1985, p. L41.

[12] S.Kang and N.J. Grant, Metall. Trans., 18A, 1987, p. 2037.

[13] H.K. Hardy and J.M. Silcock, J. Inst. of Met., 84, 1955-56, p. 423.

[14] B. Noble and G.E. Thompson, Met. Sc., 6, 1972, p. 167.

[15] J.C. Huang and A.J. Ardell, Matl. Sc. and Tech., 3, 1987, p. 176.

[16] H. Suzuki, M. Kanno and N. Hayashi, J. Jap. Inst. Light Met., 32, 1982, p. 88.

[17] R.J. Rioja and E.A. Ludwiczak in "Aluminum Alloys, Their Physical and Mechanical Properties," Vol. III, Proceedings of the International Conference on Aluminum Alloys, Chameleon Press, London, U.K., 1986, p. 471.

[18] W.A. Cassada, G.J. Shiflet and E.A. Starke, Scripta Metall., 21, 1987, p. 387.

[19] R.J. Chester and I.J. Polmear in "The Metallurgy of Light Alloys," Inst. Metall., Ser. 3, London, Vol. 20, 1983, p. 75.

[20] J.H. Auld and J.T. Vietz in "The Mechanism of Phase Transformations in Crystalline Solids," Proceedings of the International Symposium of the Institute of Metals, London, 1969, p. 77.

[21] K.M. Knowles and W.M. Stobbs, Acta Cryst., B44, 1988, p. 207.

[22] B.C. Muddle and I.J. Polmear, Acta Metall., 37, 1989, p. 777.

[23] S. Kerry and V.D. Scott, Met. Sc., 18, 1984, p. 289.

[24] A. Garg, Y.C. Chang and J.M. Howe, Scripta Metall. et Mat., 24, 1990, p. 677.

[25] B.A. Shollock, C.R.M. Grovenor and K.M. Knowles, Scripta Metall. et Mat., 24, 1990, p. 1239.

[26] D. Khireddine, R. Rahouadj and M. Clavel, Scripta Metall., 22, 1988, p. 167.

[27] R.N. Wilson and P.G. Partridge, Acta Metall., 13, 1965, p. 1321.

[28] H. Watanabe and E. Sato, J. of Japan Inst. Light Metals, 31, 1981, p. 64.

[29] A.K. Gupta, P. Gaunt and M.C. Chaturvedi, Philos Mag. A., 55, 1987, p. 375.

[30] X. Xiaoxin and J.W. Martin, J. de Physique, Calloque C3, Vol. 48, 1987, p. 433.